

Modeling the role of riverine organic matter in hypoxia formation within the coastal transition zone off the Pearl River Estuary

Liuqian Yu ,^{1,2} **Jianping Gan** ,^{1,2,3*} **Minhan Dai**,⁴ **Chiwing Rex Hui**,^{1,2} **Zhongming Lu**,³ **Dou Li**²

¹Department of Mathematics, The Hong Kong University of Science and Technology, Hong Kong, China

²Department of Ocean Science, The Hong Kong University of Science and Technology, Hong Kong, China

³Division of Environment and Sustainability, The Hong Kong University of Science and Technology, Hong Kong, China

⁴State Key Lab of Marine Environmental science, Xiamen University, Xiamen, China

Abstract

Globally expanding hypoxia in estuaries and coastal oceans has largely been attributed to the elevated river nutrient inputs, whereas the role of river-delivered terrestrial organic matter (OM_{terr}) in hypoxia formation has been less investigated. This study uses a coupled physical-biogeochemical model and observations to investigate how OM_{terr} directly (via remineralization) and indirectly (via the nutrients released from OM_{terr} remineralization) promotes hypoxia development in the coastal transition zone off the Pearl River Estuary. Results show that direct contribution of OM_{terr} remineralization to total oxygen consumption by terrestrial and marine organic matter negatively correlates with salinity, decreasing from over 60% in the upper estuary to nearly 0% in the far reaches of the river plume, and is higher in the upstream (average 30%) than the downstream region (average 18%). Nevertheless, the nutrients released from OM_{terr} remineralization greatly sustain an indirect contribution to oxygen depletion and hypoxia formation downstream. The increasing relative importance of indirect over the direct effect of OM_{terr} to hypoxia along the plume path is a combined result of the wind-driven eastward shelf current and the OM_{terr} -released nutrients being advected farther downstream than the sinking OM_{terr} . This highlights that without including the indirect effect of OM_{terr} may underestimate the role of OM_{terr} in hypoxia formation in aquatic systems. Examinations of the hypoxia response to varying riverine loads further suggest that reducing the nutrient and OM_{terr} loads is required for hypoxia mitigation in the upstream region while reducing the nutrient load alone is more effective in mitigating hypoxia in the downstream.

Hypoxia, typically defined as dissolved oxygen concentration less than 2 mg L^{-1} , has been drastically expanding in the world's estuarine and coastal waters for the past few decades, damaging the structure and function of important aquatic ecosystems (Diaz and Rosenberg 2008; Breitburg et al. 2018). The deteriorating hypoxic conditions in aquatic systems worldwide have largely been attributed to eutrophication resulting from elevated anthropogenic nutrient input (Conley et al. 2009; Rabalais et al. 2014). The classic paradigm is that an excessive nutrient supply to the aquatic system leads to a large amount of (autochthonous) organic matter (OM) being produced in surface waters, which sinks to the bottom waters or the sediments and is degraded there. The degradation consumes a large amount of oxygen and could lead to hypoxia if the physical supply of oxygen is concurrently restricted (Fennel and Testa 2019). As a consequence, reducing inorganic nutrient

loading has been the focus of hypoxia management and policy making (Deininger and Frigstad 2019).

Besides inorganic nutrients, the OM delivered from the terrestrial environment (terrestrial OM; OM_{terr}) can also contribute importantly to eutrophication (Nixon 2009). The role that this externally supplied OM (allochthonous OM) plays in hypoxia development, however, has been less investigated compared to the classic "nutrient-enrichment" paradigm, although it is gaining increasing attention (e.g., Wang et al. 2016; Su et al. 2017; Wang et al. 2018b). Indeed, rivers that deliver a large amount of nutrients to estuaries or coastal waters often concurrently supply a high OM_{terr} load. Examples include the Pearl River (Ni et al. 2008), Changjiang (Yangtze) River (Wang et al. 2012), Mississippi River (Bianchi et al. 2002), and multiple rivers discharging to the Baltic Sea (Stepanauskas et al. 2002). The riverine input of OM_{terr} can directly and indirectly contribute to oxygen depletion in aquatic systems. The direct contribution refers to the remineralization of OM_{terr} by heterotrophic bacteria that consumes oxygen and releases inorganic nutrients such as ammonium (NH_4) and phosphate (PO_4). The indirect contribution refers to the oxygen

*Correspondence: magan@ust.hk

Additional Supporting Information may be found in the online version of this article.

consumption processes fueled by the inorganic nutrients released from OM_{terr} remineralization (i.e., the aerobic oxidation of OM_{terr}-released NH₄ to NO₃ via nitrification, and remineralization of the autochthonous OM newly produced from the OM_{terr}-released nutrients).

A quantitative understanding of the relative importance of river nutrient and OM inputs in generating and maintaining hypoxia is crucial for understanding the mechanism behind hypoxia formation and for designing effective mitigation strategies. A case in point is the coastal transition zone neighboring the Pearl River Estuary and its adjacent shelf in the northern South China Sea (Fig. 1). The Pearl River Estuary is fed by the Pearl River, which is the second largest river in China in terms of freshwater discharge ($3.26 \times 10^{11} \text{ m}^3 \text{ yr}^{-1}$) and has nearly 80% of the discharge occurring during the wet season (April to September) (Zhao 1990). During summer, the strong seaward buoyant surface flow of the estuarine circulation converges with the prevailing southwesterly wind-driven along-shelf current in the coastal transition zone (Fig. 1b). This convergence produces a stable water column and long residence time that allows the large nutrient input (e.g., dissolved inorganic nitrogen, DIN, of $3.9 \times 10^5 \text{ t yr}^{-1}$) (Cai et al. 2004) and OM input ($9.2 \times 10^5 \text{ t yr}^{-1}$) (Ni et al. 2008) from the Pearl River to accumulate and promote hypoxia development in the coastal transition zone (Li et al. 2020).

Since the late 1970s, rapid economic growth and urbanization in the Pearl River Delta has occurred with concurrent large increases in anthropogenic nutrient input to the Pearl River Estuary (Ma et al. 2009; Ye et al. 2012). The increase in nutrient input fuels persistent hypoxia in the upper reaches of the estuary (Dai et al. 2006), recurring algal blooms in the lower estuary (Yin 2003), and emerging seasonal hypoxia in the coastal waters off the estuary (Qian et al. 2018; Li et al. 2020). River OM_{terr} loads, consisting of OM derived from the continent, urban sewage plants, and freshwater algae (Ni et al. 2008; Ye et al. 2017), have also increased over the decades. For example, the observed biological oxygen demand, which is an indicator of the total OM amount, has been increasing at the river outlet (Liu et al. 2020). Nevertheless, the extent to which the river-delivered OM_{terr} contributes to the deteriorating hypoxia in the coastal transition zone off the Pearl River Estuary has received little attention until recently (Su et al. 2017; Zhao et al. 2020).

Utilizing a three-endmember mixing model and isotopic compositions of dissolved inorganic carbon, Su et al. (2017) highlighted the significant contribution that OM_{terr} remineralization ($\sim 35\% \pm 16\%$) makes to oxygen depletion in the lower Pearl River Estuary, contrasting with the negligible role of OM_{terr} remineralization in the hypoxic zones of the East China Sea off the Changjiang Estuary (Wang et al. 2016) and the northern Gulf of Mexico (Wang et al. 2018b). A similar relative contribution of OM_{terr} remineralization ($\sim 33\% \pm 18\%$) to oxygen depletion in the Pearl River Estuary has also been obtained by Zhao

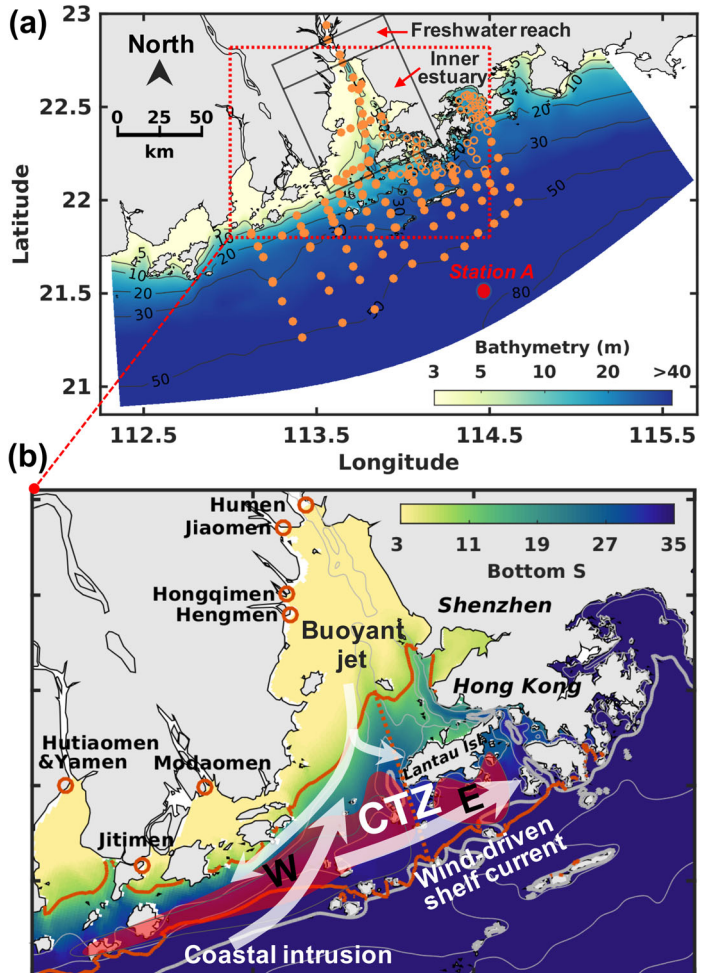


Fig. 1. (a) Model domain and bathymetry. The red dashed rectangle highlights the enlarged area shown in (b) and black rectangles denote the subregions for the spatial averages in Table 2. The orange filled and open dots denote the sampling locations during the July and August 2017 cruises, respectively. Location of Sta. A is marked with a red dot. (b) Enlarged area of the Pearl River Estuary and adjacent shelf, where the colormap shows the model-simulated bottom salinity (S) on Day 45 and red circles denote the major river outlets. The red solid lines represent the simulated bottom salinity contours of 10 (nearshore) and 34 (offshore), respectively, and the subregion within the two salinity contours are practically defined as the coastal transition zone (CTZ) used in our analysis. The red dashed line indicates the division of the western and eastern coastal transition zone, while the red areas denote the observed hypoxic centers of the 2017 cruises which fall within the coastal transition zone. White thick arrows indicate the southwestward buoyant jet, and the northeastward wind-driven shelf current with a shoreward veering component. The gray contours mark the bathymetric depths of 5, 10, 20, 30, 40, and 50 m, and a thicker gray 20 m contour.

et al. (2020) using the approach applied in Su et al. (2017). Nevertheless, these estimates are spatial averages without resolving the characteristics of the spatial variations of the relative fractions of OM_{terr} in the total OM (He et al. 2010ab; Guo et al. 2015) or the difference in contributions under different amounts of river discharge (Ye et al. 2017). These

variations are largely controlled by the OM_{terr} deposition and hydrodynamical-biogeochemical conditions along the path of the river plume, which consequently determine the relative contribution of OM_{terr} to oxygen consumption in different parts of the Pearl River Estuary. Furthermore, in addition to the above-mentioned direct contribution of OM_{terr} remineralization to oxygen consumption, the nutrients released from OM_{terr} remineralization can indirectly contribute to oxygen depletion and hypoxia by fueling nitrification and production of autochthonous OM. This indirect contribution of OM_{terr} also varies along the plume path, but its importance and variability has not been examined for this region or for any other hypoxic systems.

Coupled physical-biogeochemical models have been actively applied to identify the key processes regulating hypoxia formation in the Pearl River Estuary (Wang et al. 2017, 2018a; Lu et al. 2018). However, few of these efforts have explicitly explored the role of OM_{terr} in hypoxia formation, except for Wang et al. (2018a) who showed that the simulated hypoxia near the Modaomen river outlet on the western shelf was more sensitive to riverine OM than to nutrient input. It is also worth noting that most of the previous physical-biogeochemical models for this region were calibrated to simulate the episodic and localized hypoxia in a part of the coastal water off the Pearl River Estuary and did not integrally link to the coupled physical-biogeochemical processes in the entire estuary-shelf water system. However, long-term monthly monitoring data from 1990 to 2014 and monthly cruise surveys from the summer of 2010 have demonstrated a trend of seasonal deoxygenation and deteriorating hypoxia in the lower reach of the Pearl River Estuary (Qian et al. 2018). Additionally, repeated surveys since 2014 (Li et al. 2020) and the results presented in Fig. 1b collectively reveal the existence of hypoxia in the coastal transition zone with two distinct centers; one in the western zone and one in the eastern zone.

This study is to explicitly simulate and investigate the role that river-delivered OM_{terr} plays, relative to river nutrients, in hypoxia formation within the coastal transition zone off the Pearl River Estuary based on process-oriented numerical modeling. Specifically, we aim (1) to explore the spatial variability in the relative contribution of OM_{terr} to oxygen consumption in the coastal transition zone during a typical summer; (2) to quantify the relative importance of the direct and indirect impacts of OM_{terr} on hypoxia formation in the western and eastern coastal transition zone where two hypoxic centers locate; and (3) to investigate the relative effectiveness of reducing river nutrients and/or OM_{terr} on mitigating hypoxia in the region.

Methods

Coupled physical-biogeochemical model

Our physical numerical model is based on the Regional Ocean Modeling System (ROMS; Shchepetkin and McWilliams

2005) and was implemented and validated by Liu and Gan (2020). The model domain covers the entire Pearl River Estuary and its adjacent shelf (Fig. 1a), with an adaptive horizontal resolution that is ultrahigh (~ 0.1 km) in the estuary and inner shelf neighboring Hong Kong and gradually decreases to approximately 1 km over the shelf at the southern open boundary. It has 30 terrain-following vertical layers on S-coordinates with a higher resolution (< 0.2 m) near the surface and bottom. The model adopts the level-2.5 turbulent closure scheme developed by Mellor and Yamada (1982) for parameterizing vertical mixing, a third-order upwind-biased scheme for horizontal momentum advection, and a multi-dimensional positive-definite advection transport algorithm (MPDATA) (Smolarkiewicz and Margolin 1998) for the advection of tracers. The detailed setup and validation of the model were described in Liu and Gan (2020).

The biogeochemical module of our model is a modified version of the Nitrogen-Phosphorus-Phytoplankton-Zooplankton-Detritus model presented in Gan et al. (2014) (Fig. 2). This model was adapted from the nitrogen-based model developed by Fennel et al. (2006) to include PO₄ as an additional nutrient. A mass-conserving and computationally efficient sediment component was implemented following Fennel et al. (2006, 2011), which assumes all sinking OM that reaches the sediment-water interface to be instantly remineralized and return a flux of dissolved constituents to the bottom water, i.e., NH₄ and PO₄. This sediment treatment applies similarly to organic nitrogen and phosphorous except that a fraction of the deposited organic nitrogen is lost to nitrogen gas (N₂) through denitrification. A detailed description of the sediment parameterization is presented in Fennel et al. (2006, 2011).

For this study, we added two state variables, DOM_{terr} and POM_{terr}, to represent the terrestrial dissolved OM (operationally defined as organic particles smaller than 0.45 μ m; He et al. 2016) and particulate OM, respectively. In reality, there exist dynamic mutual exchanges between DOM and POM pools (i.e., aggregation/dissolution, adsorption/desorption, light-induced exchange, and organism-involved exchange), and these exchanges are affected by various physico-chemical and biotic factors (He et al. 2016). Considering the complexity of the exchange processes and scarcity of data to constrain the involved model parameterization, we assume an equilibrium in the exchanges between dissolved and particulate OM_{terr} pools that no exchange between them is explicitly parameterized in the model. For this simplified representation of OM_{terr} dynamics, both DOM_{terr} and POM_{terr} undergo remineralization in the water column which consumes oxygen and produces NH₄ and PO₄, while POM_{terr} can also sink to the sediment and be degraded and recycled there. Given that OM with terrestrial origins from river runoff is less labile than aquatic phytoplankton-derived OM (Guo et al. 2018; Lian et al. 2018), we implemented the following: (1) we set the remineralization rates of DOM_{terr} and POM_{terr} to an order of magnitude lower than the remineralization rate of small detritus following Yu et al. (2015);

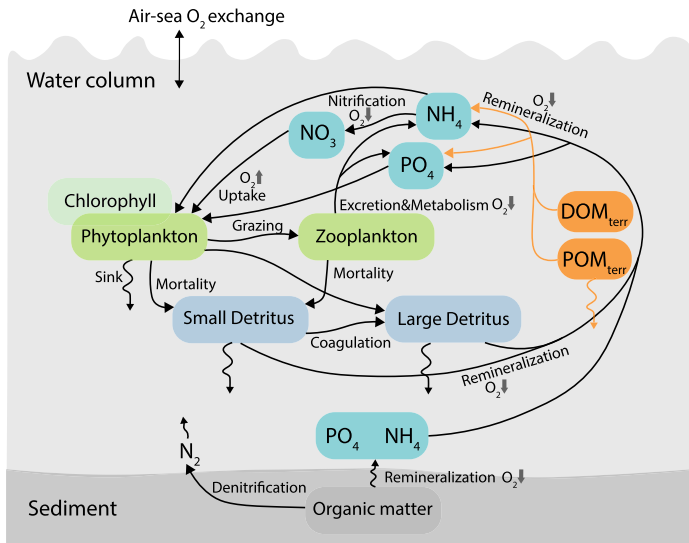


Fig. 2. Schematic of the biogeochemical model representing ecosystem processes and pathways. Biogeochemical processes that produce and consume oxygen (O_2) are indicated with up and down gray arrows, respectively. Sinking organic matter that reaches the sediment–water interface is instantly remineralized into ammonium (NH_4) and phosphate (PO_4), with a fraction of the organic nitrogen being lost to nitrogen gas (N_2) through denitrification. The acronyms NO_3 , DOM_{terr} and POM_{terr} in the schematic denote nitrate, terrestrial dissolved organic matter and terrestrial particulate organic matter, respectively.

and (2) adapted from the instantaneous remineralization treatment of autochthonous POM (i.e., marine-derived POM, POM_{mar}) at the sediment–water interface (Fennel et al. 2006, 2011), we allowed a fraction ($f_{POM_{terr}}$, set to 0.1 in the model baseline simulation) of the POM_{terr} that reached the sediment to be instantly remineralized while the rest ($1-f_{POM_{terr}}$) was returned to the bottom water layer where it could continuously be remineralized, advected, or sink. A combination of the above treatments and the adopted parameter values (Supplementary Table S1) essentially yields a higher total remineralization of the POM_{terr} than the DOM_{terr} (Table S2), consistent with the notion of higher microbial degradation of particulate than dissolved fractions of OM (Benner and Amon 2015; Attermeyer et al. 2018). Sensitivity experiments were conducted to determine the parameter values associated with OM_{terr} (Table S2), while other parameter values for the biogeochemical model (Table S1) are largely based on Gan et al. (2014) and Lu et al. (2018) but calibrated further through sensitivity experiments and comparisons against observations.

The coupled physical-biogeochemical model was employed to conduct process-oriented investigations, in which simplified but representative forcings were used in order to better distinguish the processes at work under the complex multi-forcing processes. The process-oriented approach does not attempt to reproduce observations at point-by-point sense but to explore the fundamental processes controlling system behavior, which is a necessary step to building diagnostic and

predictive models (Franks 2018). This approach has been applied and proven useful for investigating the dynamic physical (e.g., Lai and Yin 2014; Liu and Gan 2020) and biogeochemical processes (Gan et al. 2014; Lu et al. 2018), which would otherwise be difficult to achieve by using model with more realistic forcings. Following Lu et al. (2018), we applied a steady and spatially uniform southwesterly (upwelling-favorable) wind stress (0.025 Pa) over the entire model domain to represent the typical southwesterly monsoon wind during summer (Gan et al. 2014). We prescribed solar radiation with a diurnal cycle, following Gan et al. (2014), to obtain a daily average of 195 W m^{-2} for the biological module, and neglected the other buoyancy fluxes from the atmosphere. River discharge was set to a constant of $18,400 \text{ m}^3 \text{ s}^{-1}$ based on long-term river discharge summer monitoring data. Temperature (28.6°C), salinity (3 PSU, as affected by tidal intrusion into the inner estuary), and concentrations of nutrients ($90, 6$, and 1.5 mmol m^{-3} for NO_3 , NH_4 , and PO_4 , respectively) and oxygen ($O_2, 90 \text{ mmol m}^{-3}$) in the river water were adopted based on historical data and the ranges that Cai et al. (2004) estimated, while POM_{terr} and DOM_{terr} concentrations were computed from the river particulate organic carbon and dissolved organic carbon loads that Ni et al. (2008) estimated. Specifically, a carbon-to-nitrogen (C/N) ratio of 8, estimated by Ni et al. (2008), was used to convert the river OM_{terr} concentrations from C to N units, and Redfield (16 : 1) was adopted as the nitrogen-to-phosphorus (N/P) ratio of the OM_{terr} .

Profiles of temperature, salinity, NO_3 , PO_4 , O_2 , and chlorophyll measured at a far-field Sta. A (Fig. 1a) were used to generate horizontally uniform initial conditions for the model. Initial values for other unobserved variables (i.e., phytoplankton, zooplankton, and detritus) were computed using chlorophyll data and the empirical ratios between these variables and chlorophyll from Gan et al. (2014). At the open boundaries, we used a novel open boundary condition developed by Liu and Gan (2016) that concurrently accommodates tidal and subtidal forcing. The external subtidal flows were obtained from an idealized cross-shelf two-dimensional model following Gan and Allen (2005), and major tidal constituents (M2, S2, K2, N2, K1, O1, Q1, P1, and M4) were extracted from the Oregon State University Tidal Inversion Software (OTIS) (Egbert and Erofeeva 2002). A passive radiation condition was adopted for biological variables at all three open boundaries.

Model simulations

To conduct the process-oriented investigation, we ran the model for 45 d. The model reached a quasi-steady state in about 30 d (Supplementary Fig. S1, and spatial distribution of model fields on Day 30 are presented in Fig. S2). Model analysis is mainly based on results averaged over a full spring-neap tidal cycle from Day 38 (during neap tide) to Day 45 (during spring tide) and focuses on the coastal transition zone. The coastal transition zone is practically defined as the region

bounded by the model-simulated bottom salinity contours of 10 and 34 (Fig. 1b). This model simulation is referred to as the baseline case. Multiple groups of sensitivity experiments in relation to the baseline (Table 1) were conducted to examine how perturbing the river OM_{terr} and/or nutrient loads, freshwater discharge, and parameters associated with OM_{terr} (i.e., C/N ratio, POM_{terr} sinking rate, remineralization rate, and fraction of POM_{terr} being instantly remineralized in the sediment) affect hypoxia formation and the contribution of OM_{terr} to hypoxia in the coastal transition zone. Specifically, we investigate the sensitivity of hypoxia and OM_{terr} contribution to the OM_{terr} C/N ratio in the “C/N13.3” case, where a C/N ratio of 13.3 is adopted for OM_{terr} based on estimates of the terrestrial OM composition from other studies (Yu et al. 2010; He et al. 2010a). Case C/N13.3 represents the scenario of a larger fraction of land-derived OM that has a typically higher C/N ratio than OM from aquatic algae.

To distinguish between the direct and indirect contributions of OM_{terr} to the oxygen dynamics and to isolate the different processes, we conducted four additional experiments (Table 1). For two of these cases, we isolated direct contribution of OM_{terr} by turning off nutrients released from OM_{terr}

remineralization; these two cases are called “OM_{terr}_Dir only” and “C/N13.3 OM_{terr}_Dir only.” In the other two cases, we isolated indirect contribution of OM_{terr} by turning off oxygen consumption during OM_{terr} remineralization and refer to them as “OM_{terr}_Ind only” and “C/N13.3 OM_{terr}_Ind only.”

Field observations

We used a dataset from two field surveys to identify the key ecosystem features and hypoxia distribution during summer, and to validate the model results. We conducted the surveys in the Pearl River Estuary and over the adjacent shelf from 11 to 21 July 2017, and off Hong Kong from 12 to 19 August 2017 (Fig. 1a). Both surveys collected *in situ* temperature, salinity, nutrients, chlorophyll, and dissolved oxygen at different depths, with measurement techniques detailed in Li et al. (2020). During the surveys, the winds were predominated by the southwesterly upwelling-favorable wind but punctuated with episodic southeasterly downwelling-favorable wind events. The upwelling predominantly characterized the circulation as a result of the background circulation over the shelf that was set up by the flow-topography interaction (Gan et al. 2015).

Table 1. Model experiments.

Experiment	Description
Baseline	Baseline case with idealized forcing described in the Coupled physical-biogeochemical Model section.
Response to river forcing	
River OM _{terr} runs	Same as the baseline case except for increasing or decreasing dissolved and particulate terrestrial organic matter (DOM _{terr} and POM _{terr}) concentrations in river input by 25%, 50%, 75%, or 100%. “w/o OM _{terr} ” is the case representing the 100% decrease of DOM _{terr} and POM _{terr} concentrations (i.e., DOM _{terr} and POM _{terr} concentrations are 0)
River nutrient runs	Same as the baseline case except for increasing or decreasing nutrient (i.e., nitrate, ammonium, and phosphate) concentrations in river input by 25%, 50%, 75%, or 100%
River OM _{terr} and nutrient runs	Same as the baseline case except for increasing or decreasing DOM _{terr} , POM _{terr} , and nutrient (i.e., nitrate, ammonium and phosphate) concentrations in river input by 25%, 50%, 75%, or 100%
River discharge runs	Same as the baseline case except for increasing or decreasing freshwater discharge by 50%
Response to OM _{terr} physico-chemical properties	
C/N13.3	Same as the baseline case except for increasing the C/N ratio of OM _{terr} from 8 in the baseline case to 13.3
POM _{terr} sinking runs	Same as the baseline case except for changing the sinking rate of terrestrial particulate organic matter (POM _{terr}) from 5 m d ⁻¹ in the baseline case to 1, 3, 7, or 10 m d ⁻¹
POM _{terr} remineralization runs	Same as the baseline case except for increasing or decreasing the POM _{terr} remineralization rate by 50%
POM _{terr} sediment instant remineralization runs	Same as the baseline case except for increasing or decreasing the fraction of POM _{terr} being instantly remineralized in the sediment by 50%
Response to turning off indirect or direct contribution of OM _{terr}	
OM _{terr} _Dir only	Same as the baseline case except for turning off the OM _{terr} indirect contribution (i.e., no nutrients released during OM _{terr} remineralization)
OM _{terr} _Ind only	Same as the baseline case except for turning off the OM _{terr} direct contribution (i.e., no oxygen consumption during OM _{terr} remineralization)
C/N13.3 OM _{terr} _Dir only	Same as the C/N13.3 case except for turning off the OM _{terr} indirect contribution
C/N13.3 OM _{terr} _Ind only	Same as the C/N13.3 case except for turning off the OM _{terr} direct contribution

Table 2. A comparison between the model-simulated and observed total organic matter (OM) concentration and fraction of terrestrial OM (OM_{terr}) at the sediment surface. Values are spatially averaged over the freshwater reach and inner estuary (Fig. 1a) and presented as the mean \pm SD. Number of observations, n , used in the calculation is in parentheses.

		Model	Observation
Total OM concentration (mmol C m ⁻³)	Freshwater reach	232 \pm 44*	265 \pm 20 (n =2) \dagger
	Inner estuary	138 \pm 59*	136 \pm 20 (n =24) \dagger
Fraction of OM_{terr} in the inner estuary (%)		68 \pm 28	64 \pm 15 (n =10) \ddagger

*Model-simulated total OM concentration is converted from N to C units to compare with observations that are only available in C units.

\dagger Retrieved from Li et al. (2018). Data was collected in July 2015. The “Freshwater reach” corresponds to Li et al.’s “Upper Pearl River Estuary”, while “Inner estuary” corresponds to the combination of their “Middle Pearl River Estuary” and “Lower Pearl River Estuary < 5 m”.

\ddagger Retrieved from He et al. (2010a). Data was collected in May 2001. The subregion “Inner estuary” corresponds to He et al.’s “Lingdingyang Bay.”

Results

Characteristic ecosystem responses

Forced by the wind-driven shelf current, the freshwater discharge from the Pearl River flows eastward and forms a large freshwater plume stretching over the coastal transition zone as shown by the observed and simulated surface salinity (Fig. 3a,d). The freshwater is asymmetrically distributed with more accumulating over the western shelf than over the eastern shelf (Fig. 3a,d) because of the Coriolis effect and the location of major river outlets on the northwest shore (Fig. 1b). The spatial distribution of the observed and simulated surface NO_3^- (Fig. 3b,e) largely mirrors that of the freshwater plume and closely resembles the conservative mixing along the plume except for a drawdown of NO_3^- due to biological uptake at intermediate salinities (Fig. 4a). The observed and simulated surface PO_4^{3-} concentrations show a clear estuary-shelf gradient, which are replete within the inner estuary under the strong river influence but are nearly depleted at the farther edge of the plume on the shelf (Supplementary Fig. S3). Expectedly, the high-nutrient freshwater plume stimulates high surface chlorophyll concentrations throughout the coastal transition zone (Fig. 3c,f) where the stable water column and relatively low turbidity (higher light availability) favor phytoplankton growth (Lu and Gan 2015).

The observed and simulated bottom hypoxic zones are largely within the coastal transition zone with two distinct low dissolved oxygen centers in the western (upstream) and eastern (downstream) parts of the transition zone (Fig. 5a,b). Here the upstream and downstream are defined based on the direction of the eastward shelf current depicted in Figs. 1b, 3d. Vertically along the transects, the two centers are characterized with a low-oxygen layer of approximately 5 m thickness in the western and eastern parts of the transects, and these two centers are separated by relatively high oxygen in a deep channel (Fig. 5c,d). The distribution of salinity where hypoxia was observed further supports the existence of two distinct hypoxia centers, one in the lower salinity range and the other in the intermediate to high salinity range (Fig. 4b). This pattern is captured well by the simulated probability of salinity in

the hypoxic waters that shows an obvious bimodal distribution (Fig. 4b).

There exist some differences between the observations and the model results. For example, the horizontal extent of the plume and the quantitative response of the ecosystem differ between the observations and the model simulation (Fig. 3). The differences are due, for the most part, to the steady wind forcing and river discharge that we adopted for this process-oriented modeling study. Nevertheless, the model qualitatively reproduces the key observed physical-biogeochemical response to the river discharge and wind-driven shelf current. The model also captures well the observed patterns and characteristics of the hypoxic waters, which gives us confidence to continue using the model to investigate the role of OM_{terr} in promoting hypoxia formation in the coastal transition zone and the underlying mechanisms.

OM_{terr} distribution and its contribution to hypoxia

In this section, we examine the spatial distribution of OM_{terr} (combined POM_{terr} and DOM_{terr}) and quantify the direct and indirect contributions of OM_{terr} to hypoxia formation. Figure 6a shows that the surface OM_{terr} distribution essentially mirrors the distribution of the freshwater plume. The surface OM_{terr} gradually decreases from the river mouth seaward along the path of the freshwater (Fig. 6a), and the bottom OM_{terr} extends less than the surface OM_{terr} , decreasing sharply from the river mouth seaward to the 20 m bathymetric contour (Fig. 6b). The along-estuary transect of OM_{terr} concentration shows that OM_{terr} is vertically homogeneous over most of the upper estuary (Fig. 6c). OM_{terr} declines seaward (at a higher rate in the lower layers) to form a seaward surface tongue (Fig. 6c) in response to the seaward-landward two-layer estuarine circulation. A substantial amount of OM_{terr} enters the coastal transition zone from the river outlets located in the upper estuary and the western coastal transition zone (Fig. 1b). This results in gradually decreasing OM_{terr} concentrations from west to east along the along-shore section (Fig. 6d), following the path of the plume.

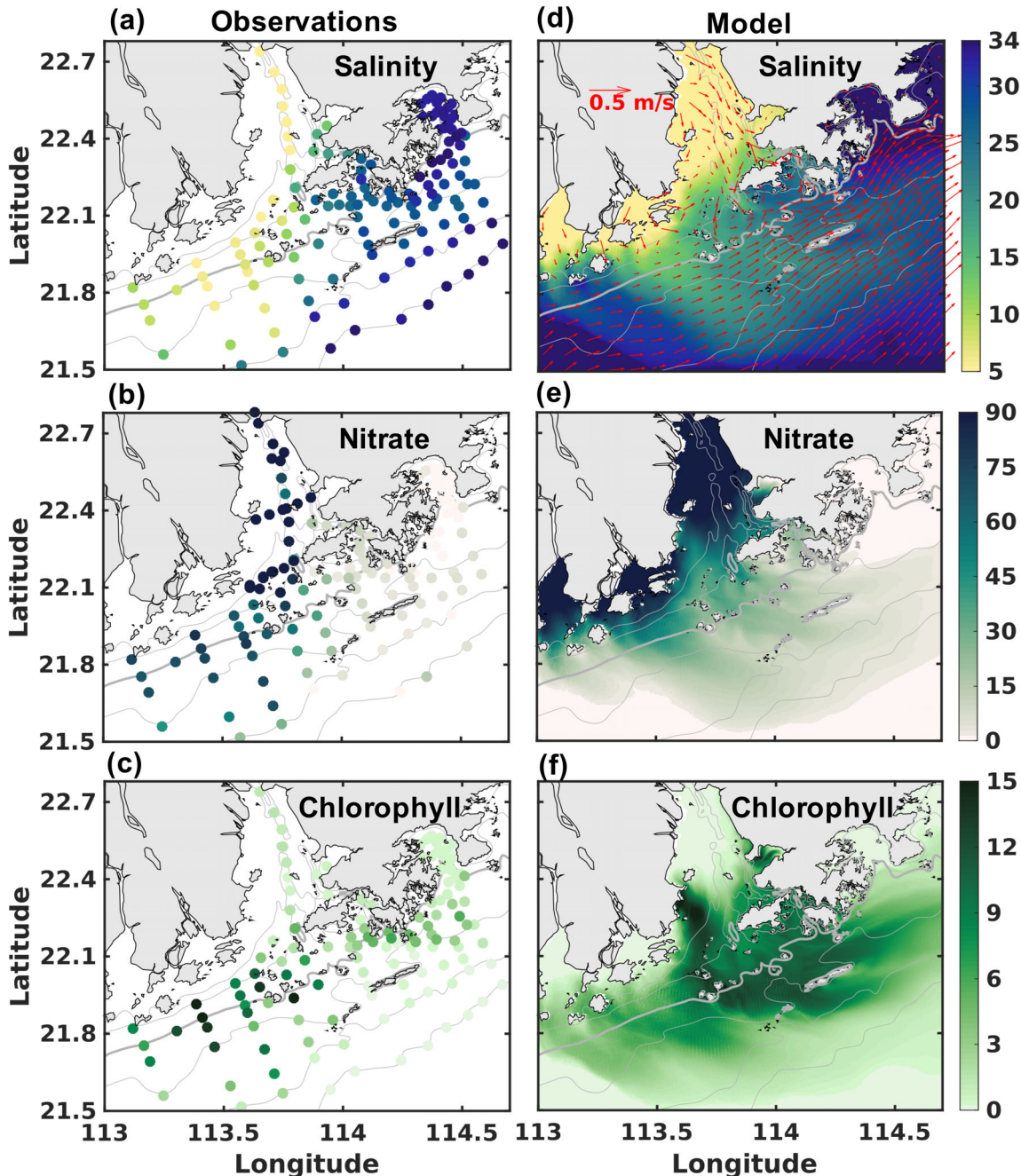


Fig. 3. (a-c) Observed and (d-f) simulated surface salinity, nitrate (mmol m^{-3}), and chlorophyll (mg m^{-3}). Simulated depth-averaged velocity vectors are superimposed onto the surface salinity in (d). The gray contours mark the bathymetric depths of 5, 10, 20, 30, 40, and 50 m, and a thicker gray 20 m contour line.

Due to the scarcity of OM data for distinguishing terrestrial OM from marine OM (OM_{mar}), we could only compare the simulated and observed ranges of the regionally averaged total OM concentrations (combined OM_{terr} and OM_{mar}) and the fraction of OM_{terr} in the total OM. Table 2 shows that the simulated total OM concentrations are within the variability range that Li et al. (2018) observed and agree with the

observed spatial gradient of higher averaged OM concentration in the freshwater reach of the Pearl River Estuary, where OM_{terr} predominated, than in the inner estuary (see Fig. 1a for location of subregions). Table 2 also shows that the simulated fraction of OM_{terr} at the sediment surface in the inner PRE is, on average, $68\% \pm 28\%$, which is also within the $64\% \pm 15\%$ range that He et al. (2010a) observed.

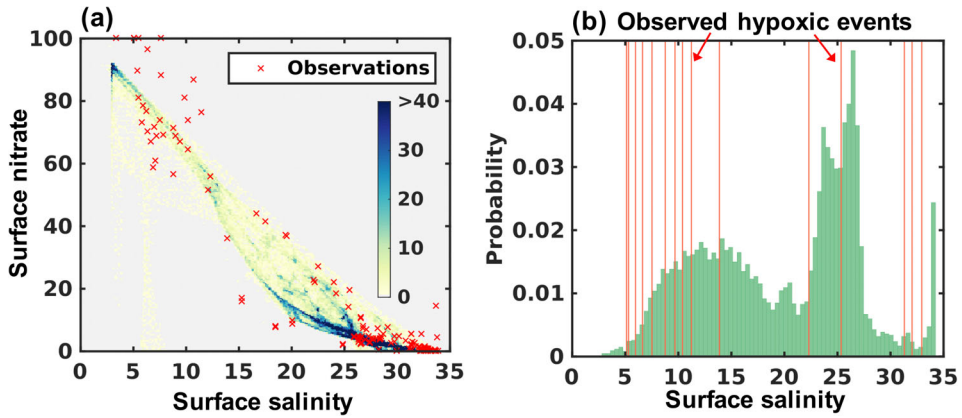


Fig. 4. (a) Surface nitrate (mmol m^{-3}) as a function of surface salinity. The color denotes the number of sampling points from the model and the red symbols represent the observed nitrate. (b) Probability distribution of the simulated surface salinity in the hypoxic waters. Red vertical lines indicate the surface salinity values where the observed hypoxic events occurred.

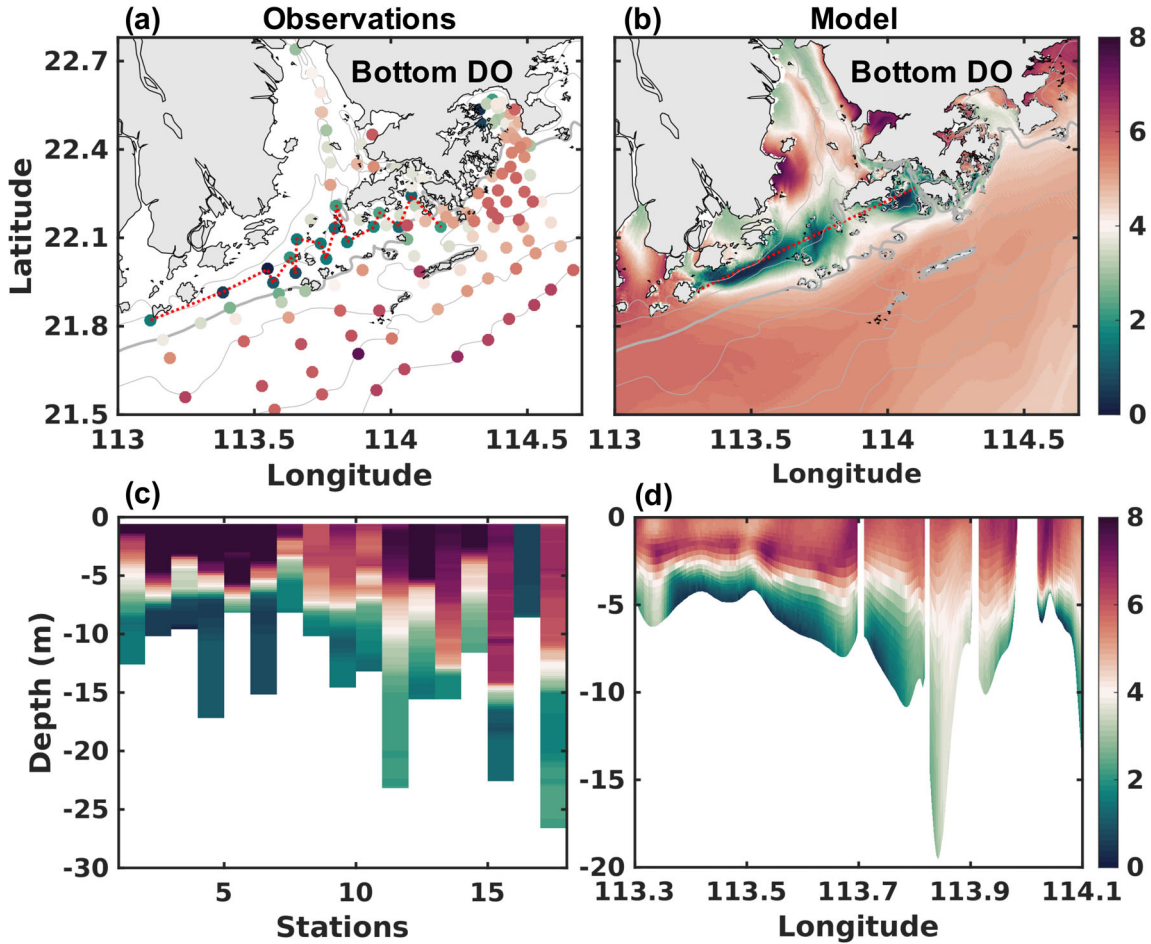


Fig. 5. (a) Observed and (b) simulated bottom dissolved oxygen (DO, mg L^{-1}). The red dashed line denotes the location of the transects. The gray contours mark the bathymetric depths of 5, 10, 20, 30, 40, and 50 m, and a thicker gray 20 m contour line. (c) Observed and (d) simulated dissolved oxygen transects along the red dashed lines depicted in (a) and (b), respectively.

Direct contribution of OM_{terr}

To assess the direct contribution of OM_{terr} to oxygen depletion and to compare that with the OM_{mar} contribution, we calculated

the vertically integrated oxygen consumption associated with each OM origin in the bottom 5 m (Fig. 7). Here, the OM_{terr} -induced oxygen sink consists of the OM_{terr} remineralization in

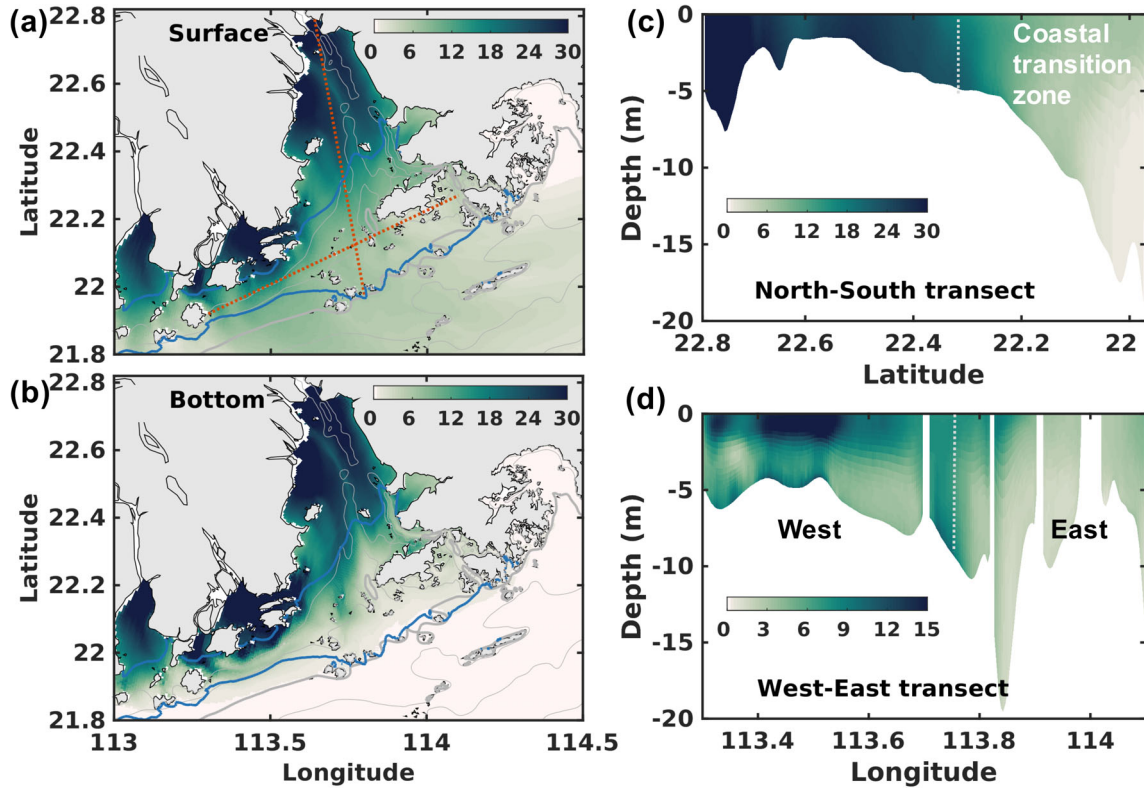


Fig. 6. (a, b) Spatial distribution of simulated surface and bottom terrestrial organic matter (OM_{terr} , mmol N m^{-3}). The red dashed lines denote the locations of the transects in the right panels. Gray contours mark the bathymetric depths of 5, 10, 20, 30, 40, and 50 m, and a thicker gray 20 m contour line. The blue solid lines depict the coastal transition zone, bounded by the simulated bottom salinity contours of 10 (nearshore) and 34 (offshore). (c) Distribution of OM_{terr} along the along-estuary (North–South) transect and (d) the along-shore (West–East) transect. The white dashed lines denote the northern boundary of the coastal transition zone in panel (c) and the division between the western and eastern coastal transition zone in (d).

the sediment and the water column, whereas the OM_{mar} -induced oxygen sink is the sum of the sediment oxygen consumption, caused by degrading phytoplankton and detritus, and the oxygen consumption in the water column caused by nitrification, zooplankton metabolism, and detritus remineralization.

As shown in Fig. 7a, the spatial distribution of the OM_{terr} oxygen sink largely follows that of the bottom OM_{terr} , declining seaward from almost 120 mmol m^{-2} at the river mouth to a very low level in the outer coastal transition zone where the bottom salinity exceeds 34. In contrast, the distribution of the OM_{mar} oxygen sink mirrors the surface chlorophyll distribution (Fig. 3f), which is low in the upper estuary and reaches a remarkably high level ($> 120 \text{ mmol m}^{-2}$) in the coastal transition zone (Fig. 7b). As a result, the direct contribution of OM_{terr} remineralization to total oxygen consumption ($\frac{\text{OM}_{\text{terr}} \text{O}_2 \text{ sink}}{(\text{OM}_{\text{terr}} + \text{OM}_{\text{mar}}) \text{O}_2 \text{ sink}} \times 100\%$) in the bottom 5 m peaks ($> 60\%$) in the upper estuary where the bottom salinity is less than 10 and decreases along the freshwater flow path to nearly 0% far beyond the coastal transition zone (Fig. 8a).

To better distinguish the spatial variation of the OM_{terr} direct contribution to total oxygen consumption and link the variation to the two hypoxia centers in the coastal transition zone, we separately plot the OM_{terr} direct contribution against

the bottom salinity for the western and eastern zones. The OM_{terr} direct contribution negatively correlates with the bottom salinity in the coastal transition zone (Fig. 8b,c). On average, OM_{terr} direct contribution to total oxygen consumption is higher ($\sim 30\%$) upstream in the western zone than downstream in the eastern zone ($\sim 18\%$). The OM_{terr} direct contribution, averaged over the entire coastal transition zone, is about 25% (Table 3), which is within the range of the spatial mean ($\sim 35\% \pm 16\%$) in the lower Pearl River Estuary that Su et al. (2017) estimated.

Indirect contribution of OM_{terr}

OM_{terr} contributes indirectly to the oxygen balance in the coastal transition zone through the release of nutrients from OM_{terr} remineralization in the water column and sediment. We quantify this indirect contribution as an increase in the biological oxygen source and sinks fueled by OM_{terr} -released nutrients, which we obtain from the difference between the baseline case and the case without the OM_{terr} -released nutrients ("OM_{terr}_Dir only"). Figure 9 shows that the indirect contribution leads to marked increases in the oxygen source, namely primary production, and oxygen sinks, which are dominated by sediment oxygen consumption followed by

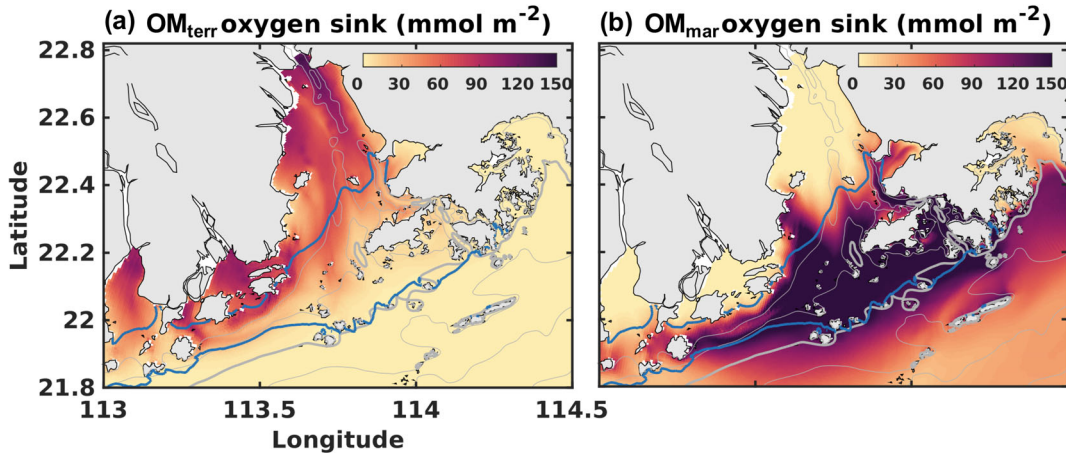


Fig. 7. Similar to Fig. 6a, but for spatial distributions of (a) terrestrial organic matter (OM_{terr}) induced and (b) marine organic matter (OM_{mar}) induced oxygen sink integrated over the bottom 5 m (including the sediment oxygen consumption).

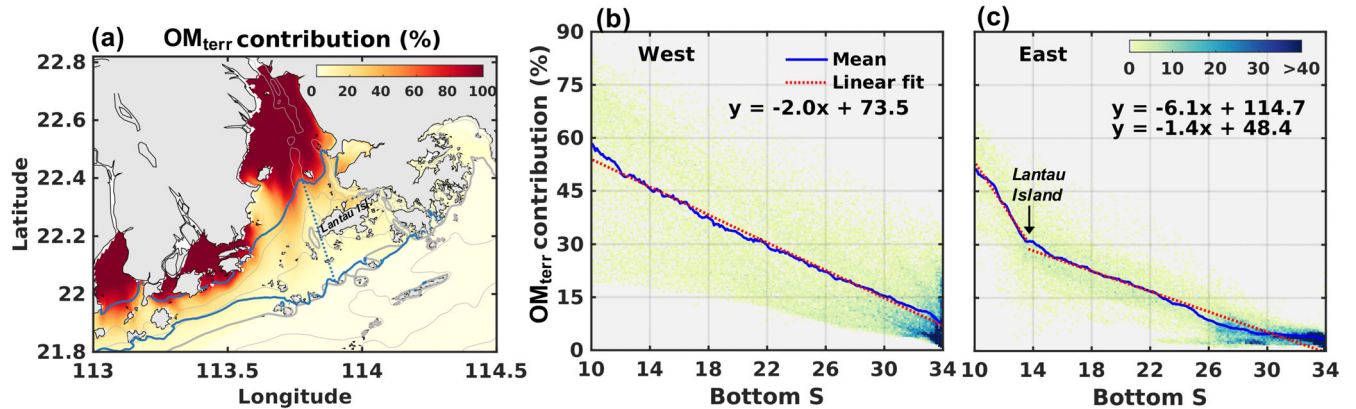


Fig. 8. (a) Similar to Fig. 6a, but for the direct contribution of terrestrial organic matter (OM_{terr}) remineralization to total oxygen consumption by terrestrial and marine (OM_{mar}) organic matter ($\frac{\text{OM}_{\text{terr}} \text{ O}_2 \text{ sink}}{(\text{OM}_{\text{terr}} + \text{OM}_{\text{mar}}) \text{ O}_2 \text{ sink}} \times 100\%$) in the bottom 5 m. (b, c) Direct contribution of OM_{terr} as function of the bottom salinity (S) in the western and eastern coastal transition zone, with the two zones divided by the thin blue dashed line shown in panel (a). Color denotes the number of sampling points. The blue solid line represents the salinity-binned OM_{terr} contribution (i.e., the mean contribution at 0.1 PSU salinity intervals). The red dashed line represents the linear fit between the OM_{terr} contribution and bottom salinity, with linear regression equations in the top right corner. In panel (c), two fitting functions are given for sampling points located at the north and south of Lantau Island, respectively.

nitrification, in the western and eastern coastal transition zone. It follows that the majority of the OM_{terr} -released nutrients are taken up by phytoplankton to refuel the originally high autochthonous OM production and the subsequent remineralization in the sediment that draws down oxygen in the bottom water.

In the western coastal transition zone, the indirect contribution of OM_{terr} to oxygen depletion is about half the size of the direct contribution (Fig. 9a). In the eastern zone, the two contributions are comparable in size (Fig. 9b). Also worth noting is that the direct oxygen consumption by OM_{terr} remineralization in the western zone is nearly double that in the eastern zone, while the indirect effects in the two zones are more or less the same and even higher in the east in terms of production (Fig. 9). In other words, more OM_{terr} is

remineralized in the upstream western zone than in the downstream eastern zone, whereas the amount of nutrients released from OM_{terr} remineralization that fuel autochthonous OM production in each zone is comparable.

Next, we quantify the direct and indirect impacts of OM_{terr} on the extent of hypoxia (Table 3). Relative to the “w/o OM_{terr} ” case, the baseline case substantially increases the hypoxic volume in the western and eastern coastal transition zone by 251% and 204%, respectively. By turning off indirect (the “ $\text{OM}_{\text{terr}}\text{-Dir only}$ ” case) or direct (the “ $\text{OM}_{\text{terr}}\text{-Ind only}$ ” case) contribution of OM_{terr} , the increasing percentages are all reduced. Specifically, the percentage increases in “ $\text{OM}_{\text{terr}}\text{-Dir only}$ ” and “ $\text{OM}_{\text{terr}}\text{-Ind only}$ ” in the western zone are comparable (113% vs. 125%), but the former is much lower than the latter in the eastern zone (25% vs. 173%). That is, the direct

Table 3. Spatially-averaged direct contribution of terrestrial organic matter (OM_{terr}) remineralization to total oxygen consumption induced by terrestrial and marine organic matter in the bottom 5 m, and hypoxic volume (km^3) from different experiments (with percentage increase relative to the “w/o OM_{terr} ” presented in parenthesis) in the western, eastern, and entire coastal transition zone.

	Western zone	Eastern zone	Entire zone
Direct contribution of OM_{terr} remineralization to total oxygen consumption			
Baseline	30%	18%	25%
C/N13.3	31%	19%	25%
Hypoxic volume (km^3) and percentage increase relative to “w/o OM_{terr} ”			
w/o OM_{terr}	0.117	0.046	0.163
Baseline	0.411 (251%)	0.139 (204%)	0.550 (237%)
C/N13.3	0.347 (196%)	0.105 (129%)	0.452 (177%)
$\text{OM}_{\text{terr}}\text{-Dir}$ only	0.249 (113%)	0.057 (25%)	0.306 (88%)
$\text{OM}_{\text{terr}}\text{-Ind}$ only	0.264 (125%)	0.125 (173%)	0.389 (139%)
C/N13.3_ $\text{OM}_{\text{terr}}\text{-Ind}$ only	0.205 (75%)	0.091 (99%)	0.297 (82%)

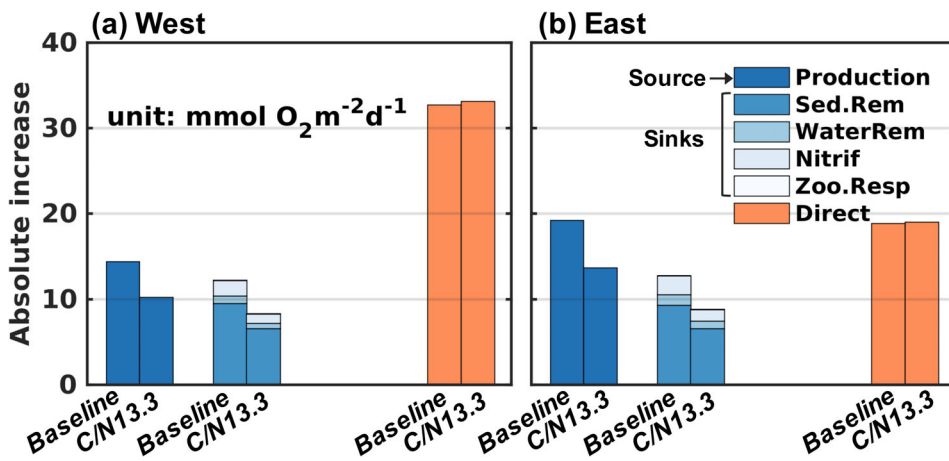


Fig. 9. Direct (orange bars) and indirect (dark to light blue bars) contributions of terrestrial organic matter (OM_{terr}) to the increase in oxygen source and sinks in the (a) western and (b) eastern coastal transition zone for the baseline and “C/N13.3” scenarios. All oxygen terms were integrated over the water column and spatially averaged over the respective zone.

and indirect contributions of OM_{terr} to hypoxia are equally important in the western zone, whereas the indirect contribution to hypoxia is much more important than the direct contribution in the eastern zone.

Spatially asymmetric response

We now examine the cause of the regional differences in the direct and indirect contributions of OM_{terr} to hypoxia. Figure 10 shows that the eastward wind-driven shelf current prevails at the surface and the bottom water. The along-shore current mostly flows eastward (Supplementary Fig. S4a), resulting in a net eastward transport of OM_{terr} -released DIN at $\sim 91 \text{ mol s}^{-1}$ and POM_{terr} at $\sim 52 \text{ mol s}^{-1}$ (Fig. S4b,c; Fig. 10). The greater eastward transport of OM_{terr} -released DIN than POM_{terr} contributes to the distinct spatial distribution pattern of the two variables, where the OM_{terr} -released DIN is more evenly distributed between the western and eastern coastal transition zone (Fig. 10a) while the POM_{terr} is more

concentrated in the western than the eastern zone (Fig. 10b). In sum, more of the POM_{terr} entering the coastal transition zone is allocated to the western than to the eastern zone (73% vs. 27%), whereas the allocation of OM_{terr} -released nutrients over the coastal transition zone is more evenly shared between the western and eastern parts (56% vs. 43% for DIN, and 60% vs. 40% for PO_4) (Supplementary Fig. S5).

Response to variable OM_{terr} physico-chemical properties and river loadings

Given that physico-chemical properties of OM_{terr} are highly variable in estuaries and coastal oceans and that strong variability exists in river freshwater and nutrient and OM loadings, we here examine how contribution of OM_{terr} to hypoxia responds to changes in these properties and river conditions.

The prescribed C/N ratio for OM_{terr} does not affect the direct oxygen consumption by OM_{terr} remineralization but affects the amount of NH_4 and PO_4 released from the remineralization,

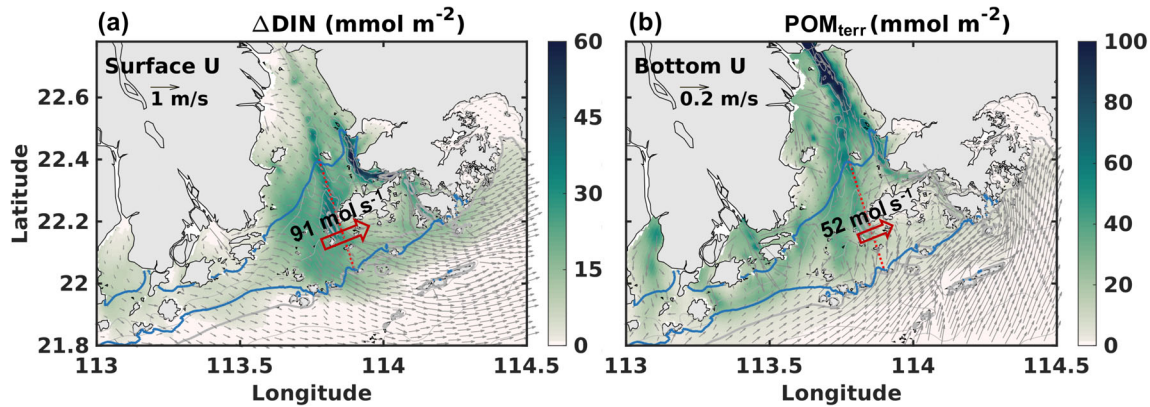


Fig. 10. (a) Spatial distribution of water-column-integrated dissolved inorganic nitrogen released by terrestrial organic matter (denoted by “ ΔDIN ”), with surface velocity vectors (U) superimposed. (b) Same as (a), but for water-column-integrated terrestrial particulate organic matter (POM_{terr}) and bottom velocity vectors. The ΔDIN and POM_{terr} were computed as the difference between the baseline case and the “w/o OM_{terr} ” case. The blue solid lines depict the coastal transition zone, and the red dashed line denotes the transect dividing the western and eastern zones. The red arrows and accompanying values denote the net eastward transport rates of ΔDIN and POM_{terr} over the entire transect.

where a higher ratio indicates less regenerated NH_4^+ and PO_4^{3-} . This effect is demonstrated by the persistently lower indirect contribution of OM_{terr} in the “C/N13.3” case than in the baseline case and nearly identical direct oxygen consumption by OM_{terr} remineralization in these two cases (Fig. 9). As a result, the indirect contribution of OM_{terr} to the increase in hypoxic volume is smaller in the “C/N13.3” case relative to the baseline case, decreasing from 125% to 75% and 173% to 99% in the western and eastern coastal transition zone, respectively. Consequently, in the “C/N13.3” case, the OM_{terr} -induced increase in hypoxic volume in the coastal transition zone decreases from 237% to 177% (Table 3).

The POM_{terr} sinking rate affects the spatial distribution of POM_{terr} (Supplementary Fig. S7) and thus the amount of POM_{terr} deposited in each part of the coastal transition zone and the allocation of POM_{terr} -released nutrients between the western and eastern zones. Generally, with increasing sinking rate, the percentage of POM_{terr} deposited in the western zone increases, while the percentage of POM_{terr} -released nutrients in the western zone also increases but to a lesser extent (Supplementary Fig. S5). Under the different sinking rates, the OM_{terr} direct contribution to total oxygen consumption varies from 19% to 30% and 13% to 19% in the western and eastern zone, respectively (Supplementary Fig. S8). Compared to the C/N ratio and sinking rate, perturbing POM_{terr} remineralization rate and fraction of POM_{terr} that is instantaneously remineralized in sediment by 50% relative to values used in the baseline case have minor impact on OM_{terr} direct contribution to oxygen consumption and hypoxic volume (Supplementary Table S2 and Fig. S8).

In both western and eastern coastal transition zone, increasing the river OM_{terr} load or the OM_{terr} plus nutrient load or the freshwater discharge lead to a simultaneous increase in the OM_{terr} contribution and the hypoxic volume,

whereas increasing the nutrient load alone decreases the OM_{terr} contribution but increases the hypoxic volume (Supplementary Fig. S8). Specifically, a 50% increase in OM_{terr} or discharge because of, for example, a typhoon event or a more intense wet season, elevates the OM_{terr} contribution to 37% or 44% in the western zone and to 23% or 32% in the eastern zone, respectively. It is also worth noting that perturbing the river discharge not only affects the biogeochemistry but also the physics. Generally, increasing or decreasing the river discharge (and hence the loading) by 50% yields a larger increase or decrease in the OM_{terr} contribution and hypoxic volume in the coastal transition zone compared to only changing the nutrient and OM loading by 50% (Fig. S8).

Response of hypoxia to changing river nutrient and OM_{terr} loads

Lastly, we investigate how the hypoxia responds to an addition or reduction in river nutrient and OM_{terr} loads (Supplementary Fig. S6 shows the simulated bottom oxygen and hypoxia distributions). Figure 11 shows that percentage changes in hypoxic volume ([experimental case – baseline]/baseline*100%) in response to changes in river nutrient and OM_{terr} loads are comparable in the western coastal transition zone (Fig. 11a), while a much more sensitive response to the changing nutrient load occurs in the eastern zone (Fig. 11b). This difference in the hypoxia response is consistent with our finding that the western zone receives more OM_{terr} than the eastern zone and that proportionally more nutrients than OM_{terr} are advected eastward following the plume path. It follows that reducing the river nutrient and OM loads is necessary for mitigating hypoxia in the western zone while reducing the nutrient load alone is more effective in the eastern zone. This is further supported by the larger hypoxia reduction when both the nutrient and OM_{terr} loads are

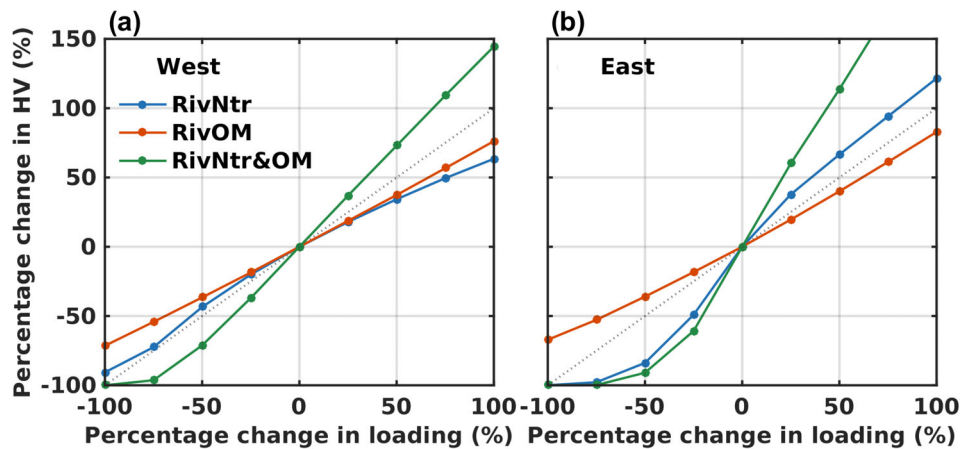


Fig. 11. Percentage change in hypoxic volume (HV) in response to the change in river nutrient (RivNtr), terrestrial organic matter (RivOM), and river nutrient plus terrestrial organic matter (RivNtr&OM) loadings in the (a) western and (b) eastern coastal transition zone. The percentage change is calculated relative to the baseline case (i.e., [experimental case – baseline]/baseline * 100%). The dashed gray line denotes the 1 : 1 ratio.

reduced in the western zone than when either load is separately reduced (Fig. 11a). In contrast, in the eastern zone, reducing both loads only yields a small additional benefit over reducing the nutrient load alone (Fig. 11b).

Discussion

By combining the field survey data from summer 2017 with the simulations from the validated process-oriented model, we show that during the wet season, biological activities in the Pearl River Estuary are determined primarily by the transport and mixing of nutrient-rich freshwater discharged from the Pearl River. The nutrient input fuels phytoplankton blooms in the coastal transition zone where the convergence of the seaward surface buoyant flow and the wind-driven along-shelf circulation creates a stable water column and a long residence time favorable for nutrient and OM accumulation. The high autochthonous OM from phytoplankton blooms and the large allochthonous OM supply from river runoff promote hypoxia formation within the coastal transition zone off the Pearl River Estuary.

Unlike the extensive investigations on the impact of anthropogenic nutrient input on hypoxia formation, the contribution of external OM supply (i.e., OM_{terr}) to oxygen depletion has received less attention in estuarine or coastal systems dominated by large rivers, including the Pearl River Estuary. By utilizing a numerical model explicitly incorporating the effects of OM_{terr} on oxygen dynamics, we estimated that the direct contribution of OM_{terr} remineralization to total oxygen consumption by terrestrial and marine OM, averaged over the coastal transition zone and a spring-neap tidal cycle during wet season, is approximately 25%, which is within the ranges that Su et al. (2017) and Zhao et al. (2020) observed. This direct contribution negatively correlates with salinity, decreasing along the path of the discharged freshwater, and thus

generating a higher (30%) contribution in the western coastal transition zone and a lower (18%) one in the eastern zone. We further show that various factors (i.e., river loadings and OM_{terr} physico-chemical properties) could affect the spatial distribution and magnitude of the direct contribution of OM_{terr}. Generally, higher river freshwater discharge, higher OM_{terr} load, lower river nutrient load, and more OM_{terr} deposition in the coastal transition zone (dependent on sinking rate of OM_{terr}) all lead to a greater relative contribution of OM_{terr} remineralization to total oxygen consumption in the coastal transition zone.

It is worth noting that the estimated direct contribution of OM_{terr} remineralization to total oxygen depletion by terrestrial and marine OM in the Pearl River Estuary is higher than that estimated in other river-dominated hypoxic systems including the East China Sea off the Changjiang Estuary (Wang et al. 2016) and the northern Gulf of Mexico (Wang et al. 2018b). The declining direct contribution of OM_{terr} along the path of Pearl River plume revealed in this study suggests that the shorter distance that the OM_{terr} travels to the hypoxic zone from the source region might be the key factor leading to the higher direct contribution of OM_{terr} in the coastal transition zone off the Pearl River Estuary. Other biogeochemical factors, including the higher bottom water temperature in the subtropical Pearl River Estuary that can accelerate the bacterial degradation of OM_{terr} (Su et al. 2017), and the higher bioavailability of OM_{terr} originating from domestic sewage effluent (Liu et al. 2020), might also play an important role and require further study.

Besides directly contributing to oxygen depletion via aerobic remineralization, OM_{terr} can also indirectly contribute to hypoxia through the nutrients it releases during remineralization. Our model results show that the released nutrients greatly fuel primary production, and the newly produced OM in turn supports high oxygen consumption in the sediment. The importance of the indirect effect of OM_{terr}

relative to the direct effect on the oxygen balance and hypoxia formation increases along the plume path. In the western coastal transition zone where major river outlets are situated, the direct and indirect effects of OM_{terr} contribute equally to the hypoxia increase, whereas downstream in the eastern zone, the indirect effect of OM_{terr} on the hypoxia dominates. This regional difference in the direct and indirect contributions of OM_{terr} to hypoxia is a combined result of the wind-driven eastward shelf current and the greater mobility of the OM_{terr}-released nutrients than the sinking OM_{terr}, which allows a larger fraction of nutrients regenerated upstream to be advected downstream to sustain oxygen depletion and hypoxia there.

The indirect contribution of OM_{terr} to hypoxia is affected by its stoichiometric C/N ratio, where a lower C/N ratio strengthens the indirect impact. A recent field study by Liu et al. (2020) showed that the organic C/N ratio in the Pearl River declines from 11.8 in the pristine upstream section to 5.0 in the estuarine section due to the abundant human-induced OM input (e.g., urban domestic sewage effluent) that has a lower C/N ratio than land-derived OM. The declining trend has also been found in the world's other large rivers such as the Changjiang (Yangtze) River and the Yellow River (Liu et al. 2020) whose receiving waters also experience hypoxia. Such a decline in the riverine organic C/N ratio further enhances the indirect effect of OM_{terr}, which makes it imperative to consider this effect when assessing contribution of OM_{terr} to oxygen dynamics and hypoxia generation.

The importance of regenerated nutrients from OM_{terr} remineralization for fueling the hypoxia development off the Pearl River Estuary, as revealed by this study, has significant implications for evaluating the role of allochthonous OM in hypoxia formation in aquatic systems. We expect that the OM_{terr} also makes an important indirect contribution to the hypoxia formation in other coastal systems. Of course, the indirect effect is largely associated with the physico-chemical properties of OM_{terr}, including the composition ratio, sinking rate, and remineralization rate that we examine in this study. Other factors like the dynamic exchange between the dissolved and particulate fractions of OM_{terr}, which could further affect the biodegradability and deposition rate of OM_{terr}, and the resuspension and burial of OM_{terr} in sediment should also be considered in future work for accurately assessing the role of OM_{terr} in hypoxia formation.

Lastly, our examination of how hypoxia responds to varying river nutrient and OM_{terr} loads suggests that, to relieve hypoxic conditions in the upstream western coastal transition zone, it is necessary to reduce both river nutrient load and OM_{terr} load. In contrast, for hypoxia mitigation downstream in the eastern zone, reducing the river nutrient load alone is more effective. The regional difference is due to the combined effects of eastward-directed coastal current and the declining OM_{terr} deposition along the coastal transition zone from upstream to downstream. This improved quantitative

understanding of the regionally different contributions of river nutrient and OM_{terr} inputs to hypoxia formation off the Pearl River Estuary can help policymakers design management plans to reduce the river nutrient and/or OM_{terr} loads and assess the effectiveness of existing strategies.

Nonetheless, caution should be taken on interpreting the model simulated reduction of hypoxia in response to changes in nutrient or OM_{terr} loading because the current model does not account for the legacy effect of the OM storage in sediments nor the sedimentary phosphorus cycling under transient redox conditions. The legacy of accumulated OM in the sediments could lead to an increase in sediment oxygen consumption from year to year despite the reduction in OM loading from overlying water after reducing river nutrient and OM_{terr} input (Turner et al. 2008). Also, the onset of hypoxia is found to increase the desorption (release) of iron-bound phosphorus from sediments that can sustain primary production in overlying waters and thus contribute to more hypoxia (Conley et al. 2002). Without credibly representing these sediment processes, the model may overestimate the speed and extent the system could recover from hypoxia following river nutrient and/or OM_{terr} loading reduction. Therefore, an important future work is to understand the impact of eutrophication legacy on hypoxia in Pearl River Estuary, as well as in other aquatic systems experiencing hypoxia, which requires more comprehensive sediment measurements and model parameterization on the deposition, resuspension, and burial of OM in seabed and the cycling of redox-sensitive elements like phosphorous in sediment. Nevertheless, the limitation in sediment parameterization of present model is considered to have little impact on our analysis focusing on the relative contributions of terrestrial vs. marine OM to hypoxia development because the limitation equally applies to all sources of OM.

Conclusions

This study explicitly quantifies the direct (remineralization) and indirect (via nutrients released from OM_{terr} remineralization) contributions of river OM_{terr} input to oxygen dynamics and hypoxia formation in the coastal transition zone off the Pearl River Estuary. We show that while the direct contribution of OM_{terr} to oxygen consumption declines along the path of plume, the nutrients released from OM_{terr} remineralization can greatly sustain an indirect contribution to oxygen depletion and hypoxia downstream following the path of plume. We suggest that not accounting for such a significant role of OM_{terr}-released nutrients in the oxygen dynamics could underestimate the importance of OM_{terr} in fueling hypoxia in estuarine and coastal ocean systems. Our work also suggest that mitigating hypoxia upstream requires reducing the river nutrient and OM_{terr} loads, and reducing the nutrient load alone is more effective for abating hypoxia downstream.

References

- Attermeyer, K., N. Catalán, K. Einarsson, A. Freixa, M. Groeneveld, J. A. Hawkes, J. Bergquist, and L. J. Tranvik. 2018. Organic carbon processing during transport through boreal inland waters: Particles as important sites. *J. Geophys. Res. Biogeosci.* **123**: 2412–2428. <http://doi.org/10.1029/2018JG004500>
- Benner, R., and R. M. W. Amon. 2015. The size-reactivity continuum of major bioelements in the ocean. *Ann. Rev. Mar. Sci.* **7**: 185–205. <http://doi.org/10.1146/annurev-marine-010213-135126>
- Bianchi, T. S., S. Mitra, and B. A. McKee. 2002. Sources of terrestrially-derived organic carbon in lower Mississippi River and Louisiana shelf sediments: Implications for differential sedimentation and transport at the coastal margin. *Mar. Chem.* **77**: 211–223. [https://doi.org/10.1016/S0304-4203\(01\)00088-3](https://doi.org/10.1016/S0304-4203(01)00088-3)
- Breitburg, D., et al. 2018. Declining oxygen in the global ocean and coastal waters. *Science* **359**: eaam7240. <https://doi.org/10.1126/science.aam7240>
- Cai, W. J., and others. 2004. The biogeochemistry of inorganic carbon and nutrients in the Pearl River estuary and the adjacent northern South China Sea. *Cont. Shelf Res.* **24**: 1301–1319. [10.1016/j.csr.2004.04.005](https://doi.org/10.1016/j.csr.2004.04.005)
- Conley, D. J., C. Humborg, L. Rahm, O. P. Savchuk, and F. Wulff. 2002. Hypoxia in the Baltic Sea and basin-scale changes in phosphorus biogeochemistry. *Environ. Sci. Technol.* **36**: 5315–5320. <http://doi.org/10.1021/es025763w>
- Conley, D. J., H. W. Paerl, R. W. Howarth, D. F. Boesch, S. P. Seitzinger, K. E. Havens, C. Lancelot, and G. E. Likens. 2009. Controlling eutrophication: Nitrogen and phosphorus. *Science* **323**: 1014–1015. <http://doi.org/10.1126/science.1167755>
- Dai, M., and others. 2006. Oxygen depletion in the upper reach of the Pearl River estuary during a winter drought. *Mar. Chem.* **102**: 159–169. <https://doi.org/10.1016/j.marchem.2005.09.020>
- Deininger, A., and H. Frigstad. 2019. Reevaluating the role of organic matter sources for coastal eutrophication, oligotrophication and ecosystem health. *Front. Mar. Sci.* **6**: 210. <https://doi.org/10.3389/fmars.2019.00210>
- Diaz, R. J., and R. Rosenberg. 2008. Spreading dead zones and consequences for marine ecosystems. *Science* **321**: 926–929. <https://doi.org/10.1126/science.1156401>
- Egbert, G. D., and S. Y. Erofeeva. 2002. Efficient inverse modeling of barotropic ocean tides. *J. Atmos. Oceanic Technol.* **19**: 183–204. [10.1175/1520-0426\(2002\)019<0183:EIMOBO>2.0.CO;2](https://doi.org/10.1175/1520-0426(2002)019<0183:EIMOBO>2.0.CO;2)
- Fennel, K., and J. M. Testa. 2019. Biogeochemical controls on coastal hypoxia. *Ann. Rev. Mar. Sci.* **11**: 105–130. [10.1146/annurev-marine-010318-095138](https://doi.org/10.1146/annurev-marine-010318-095138)
- Fennel, K., J. Wilkin, J. Levin, J. Moisan, J. O'Reilly, and D. Haidvogel. 2006. Nitrogen cycling in the Middle Atlantic Bight: Results from a three-dimensional model and implications for the North Atlantic nitrogen budget. *Global Biogeochem. Cycles* **20**: 1–14. <https://doi.org/10.1029/2005GB002456>
- Fennel, K., R. Hetland, Y. Feng, and S. DiMarco. 2011. A coupled physical-biological model of the northern Gulf of Mexico shelf: Model description, validation and analysis of phytoplankton variability. *Biogeosciences* **8**: 1881–1899. <https://doi.org/10.5194/bg-8-1881-2011>
- Franks, P. J. S. 2018. Recent advances in modelling of harmful algal blooms, p. 359–377. In *Global ecology and oceanography of harmful algal blooms*, v. **232**. Cham: Springer International Publishing. https://doi.org/10.1007/978-3-319-70069-4_19
- Gan, J., and J. S. Allen. 2005. On open boundary conditions for a limited-area coastal model off Oregon. Part 2: Response to wind forcing from a regional mesoscale atmospheric model. *Ocean Model.* **8**: 155–173.
- Gan, J., Z. Lu, A. Cheung, M. Dai, L. Liang, P. J. Harrison, and X. Zhao. 2014. Assessing ecosystem response to phosphorus and nitrogen limitation in the Pearl River plume using the Regional Ocean Modeling System (ROMS). *J. Geophys. Res. Oceans* **119**: 8858–8877. <https://doi.org/10.1002/2013JC009622>
- Gan, J., J. Wang, L. Liang, L. Li, and X. Guo. 2015. A modeling study of the formation, maintenance, and relaxation of upwelling circulation on the northeastern South China Sea shelf. *Deep-Sea Res. Part II: Top. Stud. Oceanogr.* **117**: 41–52. <https://doi.org/10.1016/j.dsr2.2013.12.009>
- Guo, W., F. Ye, S. Xu, and G. Jia. 2015. Seasonal variation in sources and processing of particulate organic carbon in the Pearl River Estuary, South China. *Estuar. Coast. Shelf Sci.* **167**: 540–548. <https://doi.org/10.1016/j.ecss.2015.11.004>
- Guo, W., G. Jia, F. Ye, H. Xiao, and Z. Zhang. 2018. Lipid biomarkers in suspended particulate matter and surface sediments in the Pearl River Estuary, a subtropical estuary in southern China. *Sci. Total Environ.* **646**: 416–426. <https://doi.org/10.1016/j.scitotenv.2018.07.159>
- He, B., M. Dai, W. Huang, Q. Liu, H. Chen, and L. Xu. 2010a. Sources and accumulation of organic carbon in the Pearl River Estuary surface sediment as indicated by elemental, stable carbon isotopic, and carbohydrate compositions. *Biogeosciences* **7**: 3343–3362. <https://doi.org/10.5194/bg-7-3343-2010>
- He, B., and others. 2010b. Distribution, degradation and dynamics of dissolved organic carbon and its major compound classes in the Pearl River Estuary, China. *Mar. Chem.* **119**: 52–64. <https://doi.org/10.1016/j.marchem.2009.12.006>
- He, W., M. Chen, M. A. Schlautman, and J. Hur. 2016. Dynamic exchanges between DOM and POM pools in coastal and inland aquatic ecosystems: A review. *Sci. Total*

- Environ. **551–552**: 415–428. <http://doi.org/10.1016/j.scitotenv.2016.02.031>
- Lai, Z., and K. Yin. 2014. Physical–biological coupling induced aggregation mechanism for the formation of high biomass red tides in low nutrient waters. *Harmful Algae* **31**: 66–75. <http://doi.org/10.1016/j.hal.2013.09.011>
- Li, X., and others. 2018. Production and transformation of dissolved and particulate organic matter as indicated by amino acids in the Pearl River Estuary, China. *J. Geophys. Res. Biogeosci.* **123**: 3523–3537. [10.1029/2018JG004690](https://doi.org/10.1029/2018JG004690)
- Li, D., J. Gan, R. Hui, Z. Liu, L. Yu, Z. Lu, and M. Dai. 2020. Vortex and biogeochemical dynamics for the hypoxia formation within the coastal transition zone off the Pearl River Estuary. *J. Geophys. Res. Oceans* **125**: 1–16. [10.1029/2020JC016178](https://doi.org/10.1029/2020JC016178)
- Lian, Z., Z. Jiang, X. Huang, S. Liu, J. Zhang, and Y. Wu. 2018. Labile and recalcitrant sediment organic carbon pools in the Pearl River Estuary, Southern China. *Sci. Total Environ.* **640**: 1302–1311.
- Liu, Z., and J. Gan. 2016. Open boundary conditions for tidally and subtidally forced circulation in a limited-area coastal model using the Regional Ocean Modeling System (ROMS). *J. Geophys. Res. Oceans* **121**: 6184–6203. [http://doi.org/10.1002/2016JC011975](https://doi.org/10.1002/2016JC011975)
- Liu, Z., and J. Gan. 2020. A modeling study of estuarine-shelf circulation using a composite tidal and subtidal open boundary condition. *Ocean Model.* **147**: 101563. [http://doi.org/10.1016/j.ocemod.2019.101563](https://doi.org/10.1016/j.ocemod.2019.101563)
- Liu, Q., Y. Liang, W. J. Cai, K. Wang, J. Wang, and K. Yin. 2020. Changing riverine organic C:N ratios along the Pearl River: Implications for estuarine and coastal carbon cycles. *Sci. Total Environ.* **709**: 136052. [http://doi.org/10.1016/j.scitotenv.2019.136052](https://doi.org/10.1016/j.scitotenv.2019.136052)
- Lu, Z., and J. Gan. 2015. Controls of seasonal variability of phytoplankton blooms in the Pearl River Estuary. *Deep-Sea Res. Part II: Top. Stud. Oceanogr.* **117**: 86–96. <https://doi.org/10.1016/j.dsr2.2013.12.011>
- Lu, Z., J. Gan, M. Dai, H. Liu, and X. Zhao. 2018. Joint effects of extrinsic biophysical fluxes and intrinsic hydrodynamics on the formation of hypoxia west off the Pearl River Estuary. *J. Geophys. Res. Oceans* **123**: 6241–6259. <https://doi.org/10.1029/2018JC014199>
- Ma, Y., W. Wei, H.-Y. Xia, B. Yu, D. Wang, Y. Ma, and L. Wang. 2009. History change and influence factor of nutrient in Lingdingyang Sea area of Zhujiang River estuary. *Acta Oceanol. Sin.* **31**: 69–76 (in Chinese).
- Mellor, G. L., and T. Yamada. 1982. Development of a turbulence closure model for geophysical fluid problems. *Reviews of Geophysics* **20**: 851–875. <https://doi.org/10.1029/RG020i004p00851>
- Ni, H. G., F. H. Lu, X. L. Luo, H. Y. Tian, and E. Y. Zeng. 2008. Riverine inputs of total organic carbon and suspended particulate matter from the Pearl River Delta to the coastal ocean off South China. *Mar. Pollut. Bull.* **56**: 1150–1157. <https://doi.org/10.1016/j.marpolbul.2008.02.030>
- Nixon, S. W. 2009. Eutrophication and the macroscope. *Hydrobiologia* **629**: 5–19. [10.1007/978-90-481-3385-7_2](https://doi.org/10.1007/978-90-481-3385-7_2)
- Qian, W., and others. 2018. Current status of emerging hypoxia in a eutrophic estuary: The lower reach of the Pearl River estuary, China. *Estuar. Coast. Shelf Sci.* **205**: 58–67. <https://doi.org/10.1016/j.ecss.2018.03.004>
- Rabalais, N., and others. 2014. Eutrophication-driven deoxygenation in the coastal ocean. *Oceanography* **27**: 172–183. [10.5670/oceanog.2014.21](https://doi.org/10.5670/oceanog.2014.21)
- Shchepetkin, A. F., and J. C. McWilliams. 2005. The regional oceanic modeling system (ROMS): A split-explicit, free-surface, topography-following-coordinate oceanic model. *Ocean Model.* **9**: 347–404.
- Smolarkiewicz, P. K., and L. G. Margolin. 1998. MPDATA: A finite-difference solver for geophysical flows. *J. Comput. Phys.* **140**: 459–480.
- Stepanauskas, R., N. O. G. Jorgensen, O. R. Eigaard, A. Zvikas, L. J. Tranvik, and L. Leonardson. 2002. Summer inputs of riverine nutrients to the Baltic Sea: Bioavailability and eutrophication relevance. *Ecol. Monogr.* **72**: 579–597. [http://doi.org/10.1890/0012-9615\(2002\)072%5B0579:SIORNT%5D2.0.CO;2](https://doi.org/10.1890/0012-9615(2002)072%5B0579:SIORNT%5D2.0.CO;2)
- Su, J., M. Dai, B. He, L. Wang, J. Gan, X. Guo, H. Zhao, and F. Yu. 2017. Tracing the origin of the oxygen-consuming organic matter in the hypoxic zone in a large eutrophic estuary: The lower reach of the Pearl River Estuary, China. *Biogeosciences* **14**: 4085–4099. <https://doi.org/10.5194/bg-14-4085-2017>
- Turner, R. E., N. N. Rabalais, and D. Justic. 2008. Gulf of Mexico hypoxia: Alternate states and a legacy. *Environ. Sci. Technol.* **42**: 2323–2327.
- Wang, X., H. Ma, R. Li, Z. Song, and J. Wu. 2012. Seasonal fluxes and source variation of organic carbon transported by two major Chinese Rivers: The Yellow River and Changjiang (Yangtze) River. *Global Biogeochem. Cycles* **26**: 1–10. [http://doi.org/10.1029/2011GB004130](https://doi.org/10.1029/2011GB004130)
- Wang, H., and others. 2016. Eutrophication-driven hypoxia in the East China Sea off the Changjiang Estuary. *Environ. Sci. Technol.* **50**: 2255–2263. <https://doi.org/10.1021/acs.est.5b06211>
- Wang, B., J. Hu, S. Li, and D. Liu. 2017. A numerical analysis of biogeochemical controls with physical modulation on hypoxia during summer in the Pearl River Estuary. *Biogeosciences* **14**: 2979–2999.
- Wang, B., J. Hu, S. Li, L. Yu, and J. Huang. 2018a. Impacts of anthropogenic inputs on the hypoxia and oxygen dynamics in the Pearl River Estuary. *Biogeosciences* **15**: 6105–6125.
- Wang, H., X. Hu, M. S. Wetzel, and K. C. Hayes. 2018b. Oxygen consumption and organic matter remineralization in two subtropical, eutrophic coastal embayments. *Environ. Sci. Technol.* **52**: 13004–13014. <https://doi.org/10.1021/acs.est.8b02971>

- Ye, F., X. Huang, X. Zhang, D. Zhang, Y. Zeng, and L. Tian. 2012. Recent oxygen depletion in the Pearl River Estuary, South China: Geochemical and microfaunal evidence. *J. Oceanogr.* **68**: 387–400. <https://doi.org/10.1007/s10872-012-0104-1>
- Ye, F., W. Guo, Z. Shi, G. Jia, and G. Wei. 2017. Seasonal dynamics of particulate organic matter and its response to flooding in the Pearl River Estuary, China, revealed by stable isotope ($\delta^{13}\text{C}$ and $\delta^{15}\text{N}$) analyses. *J. Geophys. Res. Oceans* **122**: 6835–6856. <https://doi.org/10.1002/2017JC012931>
- Yin, K. 2003. Influence of monsoons and oceanographic processes on red tides in Hong Kong waters. *Mar. Ecol. Prog. Ser.* **262**: 27–41.
- Yu, F., Y. Zong, J. M. Lloyd, G. Huang, M. J. Leng, C. Kendrick, A. L. Lamb, and W. W. S. Yim. 2010. Bulk organic $\delta^{13}\text{C}$ and C/N as indicators for sediment sources in the Pearl River delta and estuary, southern China. *Estuar. Coast. Shelf Sci.* **87**: 618–630. <http://doi.org/10.1016/j.ecss.2010.02.018>
- Yu, L., K. Fennel, A. Laurent, M. C. Murrell, and J. C. Lehrter. 2015. Numerical analysis of the primary processes controlling oxygen dynamics on the Louisiana shelf. *Bio-geosciences* **12**: 2063–2076.
- Zhao, H. 1990. Evolution of the Pearl River Estuary. Beijing: China Ocean Press, (in Chinese).
- Zhao, Y., and others. 2020. Dynamics of inorganic carbon and pH in a large subtropical continental shelf system: Interaction between eutrophication, hypoxia, and ocean acidification. *Limnol. Oceanogr.* **65**: 1359–1379. <https://doi.org/10.1002/lo.11393>

Acknowledgments

We thank two anonymous referees for their constructive comments. The ROMS code to generate the model output can be accessed at <https://www.myroms.org/>. The observational data used in this research can be downloaded from <https://ocean.ust.hk/data/>. This research was supported by the Theme-based Research Scheme (T21-602/16-R, OCEAN_HK project) of the Hong Kong Research Grants Council. We acknowledge the support of the National Supercomputer Center of Tianhe-1 (Tianjin) and Tianhe-2 (Guangzhou).

Conflict of Interest

None declared.

Submitted 05 March 2020

Revised 25 June 2020

Accepted 08 September 2020

Associate editor: Thomas Anderson